

Communication

Near-field electrospinning for 3D stacked nanoarchitectures with high aspect ratios

Yang-Seok Park, Junyoung Kim, Jung Min Oh, Seungyoung Park, Seungse Cho, Hyunhyub Ko, and Yoon-Kyoung Cho

Nano Lett., **Just Accepted Manuscript** • DOI: 10.1021/acs.nanolett.9b04162 • Publication Date (Web): 25 Nov 2019

Downloaded from pubs.acs.org on November 28, 2019

Just Accepted

"Just Accepted" manuscripts have been peer-reviewed and accepted for publication. They are posted online prior to technical editing, formatting for publication and author proofing. The American Chemical Society provides "Just Accepted" as a service to the research community to expedite the dissemination of scientific material as soon as possible after acceptance. "Just Accepted" manuscripts appear in full in PDF format accompanied by an HTML abstract. "Just Accepted" manuscripts have been fully peer reviewed, but should not be considered the official version of record. They are citable by the Digital Object Identifier (DOI®). "Just Accepted" is an optional service offered to authors. Therefore, the "Just Accepted" Web site may not include all articles that will be published in the journal. After a manuscript is technically edited and formatted, it will be removed from the "Just Accepted" Web site and published as an ASAP article. Note that technical editing may introduce minor changes to the manuscript text and/or graphics which could affect content, and all legal disclaimers and ethical guidelines that apply to the journal pertain. ACS cannot be held responsible for errors or consequences arising from the use of information contained in these "Just Accepted" manuscripts.

1
2
3
4
5
6
7
8
9
10
11
12
13
14
15
16
17
18
19
20
21
22
23
24
25
26
27
28
29
30
31
32
33
34
35
36
37
38
39
40
41
42
43
44
45
46
47
48
49
50
51
52
53
54
55
56
57
58
59
60

Near-field electrospinning for 3D stacked nanoarchitectures with high aspect ratios

Yang-Seok Park,^{1,2,+} Junyoung Kim,^{1,2,+} Jung Min Oh,^{1,2,†} Seungyoung Park,³ Seungse Cho,³ Hyunhyub Ko,³ Yoon-Kyoung Cho^{1,2,3}*

¹Department of Biomedical Engineering, School of Life Sciences, Ulsan National Institute of Science and Technology (UNIST), Ulsan 44919, Republic of Korea

²Center for Soft and Living Matter, Institute for Basic Science (IBS), Ulsan 44919, Republic of Korea

³School of Energy and Chemical Engineering, Ulsan National Institute of Science and Technology (UNIST), Ulsan 44919, Republic of Korea

*To whom correspondence should be addressed: ykcho@unist.ac.kr.

KEYWORDS: nanofiber, near-field electrospinning, multilayer, transparent electrode, 3D printing

ABSTRACT

Near-field electrospinning (NFES) was developed to overcome the intrinsic instability of traditional electrospinning processes and to facilitate the controllable deposition of nanofibers

under a reduced electric field. This technique offers a straightforward and versatile method for the precision patterning of two-dimensional (2D) nanofibers. However, three-dimensional (3D) stacked structures built by NFES have been limited to either micron-scale sizes or special shapes. Herein, we report on a direct-write 3D NFES technique to construct self-aligned, template-free, 3D stacked nanoarchitectures by simply adding salt to the polymer solution. Numerical simulations suggested that the electric field could be tuned to achieve self-aligned nanofibers by adjusting the conductivity of the polymer solution. This was confirmed experimentally by using polyethylene oxide (PEO) solutions containing 0.1–1.0 wt% NaCl. Using 0.1 wt% NaCl, nanowalls with a maximum of 80 layers could be built with a width of 92 ± 3 nm, height of 6.6 ± 0.1 μ m, and aspect ratio (height/width) of 72. We demonstrate the 3D printing of nanoskyscrapers with various designs, such as curved nanowall arrays, nano “jungle gyms,” and nanobridges. Further, we present an application of the 3D stacked nanofiber arrays by preparing transparent and flexible polydimethylsiloxane (PDMS) films embedded with Ag-sputtered nanowalls as 3D nanoelectrodes. The conductivity of the nanoelectrodes can be precisely tuned by adjusting the number of 3D printed layers, without sacrificing transmittance (98.5%). The current NFES approach provides a simple, reliable route to build 3D stacked nanoarchitectures with high-aspect ratios for potential application in smart materials, energy devices, and biomedical applications.

Electrospinning is a well-established technique for the fabrication of various types of nanofibers with different compositions and structures. Electrospun nanofibers have been used for a broad range of applications, including filtration membranes, catalysts, electronic devices, and biomedical scaffolds.¹ However, the uncontrollable nature of the electrospun jet limits the application of this technique to the fabrication of devices that do not require precisely deposited fibers.¹ In contrast, controlled nanofiber deposition can be realized by near-field electrospinning (NFES), as the bending instability of the jet is significantly reduced because the distance between the nozzle and the collector is reduced to a few centimeters (typically <5 cm), and the applied voltage is lowered to several hundred volts.^{2,3} Furthermore, the collector can be moved in the X–Y direction at a programmable speed, allowing various micro/nanopatterns of waved or straight fibers to be prepared.^{3–8}

Although NFES has various advantages, such as low-voltage deposition, precise patterning of fibers, minimum consumption of materials, and good position controllability, its use is typically limited to creating two-dimensional (2D) structures on flat surfaces.⁹ Nevertheless, three-dimensional (3D) mesh structures can be built^{10–15} by layer-by-layer additive printing by NFES using highly viscous polymer melts, as they have improved directional stability toward the grounded collector in comparison to the polymer solutions used in conventional electrospinning and NFES processes. For example, Wunner *et al.* demonstrated¹⁴ the fabrication of thick scaffold structures from micrometer-sized fibers using multilayer additive printing with a highly viscous polymer melt. To promote accurate alignment in the vertical direction, they adjusted the distance between the spinneret and the collector and increased the applied voltage to compensate for electric repulsion between the deposited polymer and successive fibers. However, highly viscous polymer

1
2
3 melts typically produce much thicker fibers (on the order of several micrometers) than those
4
5 obtained via conventional far-field electrospinning or solution-based NFES processes.^{16,17}
6

7
8 It has been demonstrated¹⁸ that nanoscale 3D structures can be fabricated by the repetitive
9
10 deposition of nanofibers onto a metal electrode on an insulating collector. However, patterning of
11
12 the conducting electrode is a prerequisite, as the shapes of the nanowalls are dictated by the
13
14 predesigned pattern on the electrode.¹⁸ Kim *et al.* reported¹⁹ a hollow pottery structure constructed
15
16 by the spontaneous coiling of electrospun nanofibers when a sharp electrode tip was positioned
17
18 underneath an insulating substrate. However, the constructed structures were limited to hollow
19
20 cylindrical shapes. Zhao *et al.* demonstrated²⁰ that the patterns of electrospun fiber mats could
21
22 replicate topographical features such as protrusions on the insulating substrate. It was shown that
23
24 the insulating substrate could be polarized upon the application of a strong external electric field
25
26 that could affect the distribution of the intrinsic electric field. Furthermore, adsorbed water
27
28 molecules²¹ or functional electrolyte patterns²² on insulating substrates or electrolyte solutions²³
29
30 could serve as conducting collector electrodes that allow the deposition of electrospun fibers. Luo
31
32 *et al.*²⁴ used printing paper as a collecting substrate, whereby the residual solvent from the
33
34 deposited fibers could wet the paper and thus connect to the grounded plate. The fibers were
35
36 selectively attracted on top of the previously deposited fibers to form 3D architectures. However,
37
38 this process required a wicking substrate, and the diameters of the fibers were relatively large (on
39
40 the order of several micrometers). In summary, to the best of our knowledge, self-aligned and
41
42 stacked 3D structures built via layer-by-layer printing by design using NFES have been limited to
43
44 the micron scale or to specific prefabricated shapes, such as hollow cylinders or nanowalls, based
45
46 on specific collector requirements. Despite the importance of low-cost, versatile, and reliable
47
48
49
50
51
52
53
54
55
56
57
58
59
60

1
2
3 methods for the controlled alignment and patterning of 3D nanostructures with high precision, the
4
5 currently available methods are rudimentary.
6

7
8 Herein, we introduce a precise direct-write 3D nanoprinting process based on NFES that can
9
10 build template-free, self-aligned, 3D stacked, and high aspect ratio nanostructures, without any
11
12 prior requirements for the collector design. By simply adding salt to the PEO solution, we could
13
14 ensure precision patterning and self-alignment in the Z-axis, with precise control of the layer-by-
15
16 layer nanofiber deposition. Using this modification, we were able to print nanowalls with
17
18 thicknesses of 92 ± 3 to 239 ± 30 nm and aspect ratios (height/width) of 48–72 depending on the
19
20 concentration of salt in the PEO solution. Various 3D nanoarchitectures were designed and created,
21
22 such as curved nanowalls, nano “jungle gyms,” and nanobridges. We then elucidated the
23
24 fundamental mechanism that enabled the spontaneous self-stacking of nanofibers on top of each
25
26 layer, and demonstrated the applicability of this technique in the field of nanoelectronics by using
27
28 the 3D printed nanowalls as templates to pattern transparent nanoelectrodes with controllable
29
30 electrical resistances.
31
32
33
34

35
36 The modified NFES process provided high resolution control of the width and height of the self-
37
38 stacked nanowalls (see **Figure 1**). NFES enables the precise deposition of a stable jet by accurately
39
40 positioning the spinneret tip a short distance from the collector. Straight nanofibers can be printed
41
42 by moving the substrate faster than the electrospinning deposition rate. Here, we 3D printed
43
44 multiple layers of nanofibers by moving the motorized stage back and forth in the Y direction (at
45
46 a fixed X and Z position).
47
48

49
50 During conventional electrospinning, a high voltage is applied to the needle of the syringe that
51
52 contains the polymer solution, and this voltage is grounded to the collector substrate. As
53
54 extensively reviewed by Collin *et al.*,²⁵ the generation of charge carriers in the polymer solution is
55
56
57
58
59
60

1
2
3 primarily determined by two processes: the direct injection of charge carriers into the liquid from
4
5 conducting materials under strong electric fields; and charge dissociation from dissolved ion pairs
6
7 that already exist in the bulk of the liquid. These mechanisms provide excess charge carriers to the
8
9 polymer solution, which accelerates the force of the jet toward a grounded collector. The charge
10
11 dissipates both in the flight phase and after deposition on the collecting electrode. The charge
12
13 dissipation mechanisms are two-fold, including a surface contact discharge and an inverse corona
14
15 discharge from the deposited fiber to the conducting substrate. However, the charge does not fully
16
17 dissipate, leaving the solidified fibers with a considerable residual charge (**Figure 1A**). As the
18
19 charged fibers accumulate on the collecting substrate, the electric field is screened. Although the
20
21 physical mechanism of charge generation in electrospun fibers is fairly well understood, the charge
22
23 dissipation mechanism of solidified fibers has not been fully elucidated.²⁵

24
25
26
27
28 We hypothesized that, by enhancing the charge dissipation through the collecting substrate, the
29
30 electric field could be focused toward the pre-deposited nanofiber, which would optimize the
31
32 electrospinning conditions. Moreover, an accelerated discharge process should enhance the self-
33
34 stacking and precision of 3D printed nanofibers. We performed finite element analyses with
35
36 COMSOL Multiphysics to identify the electric fields guiding the electrospun jets when using
37
38 conductive or non-conductive polymer solutions and substrates, as shown in **Figures 1B–1E**.
39
40 When pure PEO solution (non-conductive) was deposited on a conducting substrate (**Figure 1 (i)**),
41
42 the deposited fibers had a weak positive surface charge. Moreover, the x-component of the electric
43
44 field guiding the fiber deposition was in the repulsive direction. On the other hand, as the
45
46 conductivity of the polymer solution was increased by adding NaCl (**Figure 1 (ii)**), the surface
47
48 charge density of the deposited fibers became negative; this created an attraction between the
49
50 nanofiber stream and the previously deposited fibers. The charge dissipation was less efficient
51
52
53
54
55
56
57
58
59
60

when using an insulating substrate (**Figure 1 (iii)**), which reduced the negative surface charge density and the degree of focusing. The detailed physical parameters used in the simulation are given in the Supporting Information (**Tables S1 and S2**).

These theoretical predictions were confirmed experimentally by 3D printing nanofibers under the same conditions. When pure PEO solution was printed, the nanofibers were deposited in random X positions (**Figure 1F (i)**), probably because of the repulsive force generated between the nanofiber jet and the previously deposited fibers. Conversely, when the PEO solution contained a small amount of NaCl (0.1–1.0 wt%), 3D stacked self-aligned nanofibers were synthesized (**Figure 1F (ii)**). We expect that this self-stacking phenomenon results from the efficient charge dissipation from the deposited fiber. To confirm this hypothesis, we used an insulating substrate as the grounded collector (e.g., SiO₂ film on a silicon wafer); it was observed that the precision of the self-alignment was diminished (**Figure 1F (iii)**). However, precise self-aligned 3D printed nanoarchitectures were obtained when using various conducting substrate, including doped Si, Au, and ITO (**Figure S1**). This observation implies that charge dissipation from the deposited fibers is crucial for inducing an electrical force to accurately guide the nanofiber jet. Efficient charge dissipation dramatically increases the surface polarization, which in turn induces a higher attraction between the nanofiber jet and the deposited fiber.

The attraction between the nanofiber jet and deposited polymer was stronger at higher salt concentrations (i.e., at higher conductivities), even when the substrate was stationary (**Figure S2 and Video S1**). However, when pure PEO solution was used, the repulsive force accumulated after the fibers were deposited in a particular area, causing the jet to move to a new location. With a more conductive polymer solution, when we applied an electric field, the previously deposited fiber was strongly attracted to the Taylor cone (**Video S2**). This strong attraction was not observed

when the voltage was turned off, or when the polymer solution did not contain salt (**Video S2**), which suggests that the deposited nanofibers were negatively charged when using PEO salt solution.

We were able to construct 3D nanoarchitectures with controllable dimensions by manipulating the motion of the stage during 3D NFES to deposit the nanofibers in desired patterns, as shown in **Figures 2** and **S3**. For example, nanowalls of a desired height could be built by stacking a precise number of nanofiber layers ($R^2 = 0.97$; **Figures 2C and 2D**). The scanning electron microscopy (SEM) images in **Figure 2C** show side views of 3D nanowalls with different numbers of layers. The orderly morphology of the stacked nanolayers can be seen in detail. With a 1 wt% NaCl PEO solution, we successfully produced nanowalls comprising up to 100 nanofiber layers (height: 1.0 ± 0.2 to 11.4 ± 0.9 μm , mean thickness: 239 ± 30 nm, length: 2 cm, maximum aspect ratio (height/width): 48). The width of the 3D nanoarchitecture decreased linearly as the salt concentration decreased (**Figure 2B**), reaching 92 ± 3 nm at 0.1 wt% NaCl (height: 0.8 ± 0.1 to 6.6 ± 0.1 μm , maximum aspect ratio: 72). However, at higher NaCl concentrations (2.0 wt%), the width of the fiber was not uniform and the surface was rough; and at lower concentrations (<0.1 wt%), we could not achieve precise self-stacking. Therefore, the optimized experimental condition uses PEO solution with 0.1–1 wt% NaCl.

The self-assembly of 3D fibrous structures has been reported previously^{26–29} in conventional far-field electrospinning on account of electrostatic forces between the previously deposited material and the aerial fibers. However, the electrospun fibers were either formed into irregular 3D spongiform fiber stacks^{26,27} or peculiar honeycomb-shaped foam-like structures.^{28,29} Here, the proposed 3D nanoprinting technique could create various “nanoskyscraper” designs using preprogrammed X–Y stage motion. Once built, the 3D printed polymer nanoarchitectures could

be stably coated with functional materials (e.g., Ni, Au, SiO₂, and ZnO). To demonstrate the versatility of this process, we produced straight Ni nanowall arrays, curved Au nanowall arrays, and SiO₂ nanojungle gyms from 40-layer high nanowalls (mean height: $3.2 \pm 0.3 \mu\text{m}$, mean thickness: $239 \pm 30 \text{ nm}$), and produced ZnO nanobridges by suspending single fibers on top of two such nanowalls. The structures were analyzed by SEM and energy dispersive X-ray spectroscopy (EDS), as shown in **Figures 3 and S5**. When 1.0 wt% NaCl PEO solution was used, the 3D nanowalls could be built at a distance of 25–100 μm from each other (**Figure S4**). When the pitch was less than 25 μm , the stacked fibers were misaligned owing to electrostatic interference from the nearby 3D structures.

To demonstrate a potential application of the nanoarchitectures built by the proposed NFES method, nanowalls with high aspect ratios were sputtered with Ag and used as a template to prepare transparent and flexible PDMS substrates embedded with 3D nanoelectrodes. As shown in **Figure 4A**, the 3D nanowall arrays were initially sputtered with Ag (100 nm), followed by the deposition of an anti-adhesive coating. After PDMS casting, the PDMS film and embedded 3D Ag nanowires were gently detached from the substrate. The anti-adhesive coating played an important role in separating the PDMS layer from the substrate. The presence of Ag nanowires with a width of 400 nm and height of $3.3 \pm 0.3 \mu\text{m}$ embedded in the PDMS film was further confirmed by SEM–EDS analyses (**Figures 4B–4F and S6**).

The optical and electrical properties of the 3D Ag nanowire-embedded PDMS film were then characterized. As shown in **Figure 5A**, the electrode is highly transparent; the “UNIST” letters are clearly visible through the film. The transmittance in the visible wavelength was maintained at ~98.5% (**Figure 5B**). Moreover, irrespective of the wavelength, high-transmittance values (98–99%) were attained for transparent electrodes with embedded 3D Ag nanowires of different heights

(**Figure S7**). To analyze the electrical properties, transparent electrodes were prepared using arrays of ten 3D printed nanowires of various heights (20–100 layers) and a pitch of 50 μm . The current–voltage (I–V) curves of the transparent electrodes (**Figure 5C**), obtained under direct current (DC) voltage sweeping mode from -4 V to 4 V , yielded a stable ohmic contact. The electrical resistance, sheet resistance, and resistivity were estimated from the measurements, and are listed in **Table S3**. As shown in **Figure 5D**, the electrical resistance and sheet resistance could be precisely tuned ($323\text{--}756\ \Omega$ and $7\text{--}17\ \Omega\ \square^{-1}$, respectively) depending on the number of 3D printed nanofiber layers (40–100 layers). The expected data in **Figure 5D** are based on calculations according to the measured dimensions (given in **Table S3**) and the resistivity of 3D printed Ag microstructures reported by An *et al.*³⁰ Based on the measurements of the resistance and the dimensions of the 3D Ag nanowires, the average resistivity of the transparent electrode was calculated to be $3 \times 10^{-7}\ \Omega\ \text{m}$. This value is comparable to those of 3D printed Ag structures prepared by inkjet printing ($3 \times 10^{-7}\ \Omega\ \text{m}$)³⁰ and 2D printed Ag ink ($2 \times 10^{-7}\ \Omega\ \text{m}$).³¹ In contrast, the electrodes prepared from 3D stacked nanofibers with 40–100 layers (heights of 3.3 ± 0.3 to $11.5 \pm 1.0\ \mu\text{m}$) showed excellent agreement to the expected values (**Figure 5D**), while the 3D Ag electrode prepared from 20-layer high nanowires (height: $\sim 2.4 \pm 0.2\ \mu\text{m}$) yielded an abnormally high resistance. As we investigated the morphologies of 3D Ag nanowires—unlike the Ag nanowires with higher aspect ratios—the 20-layer high Ag nanowires had fluffy and partially damaged edges, as indicated by the yellow arrows in **Figure S8**. We believe this could be attributed to weak adhesion between the PDMS layer and the 3D Ag nanowire. Nevertheless, this demonstrates the importance of the high aspect ratio of the 3D nanoarchitecture.

It is remarkable that this simple, clean-room-free process can provide such excellent tunability and reproducibility of the electrical resistance of the 3D transparent nanoelectrode. The robust and

precise control of the electrical resistance was further validated by comparing the light intensity of light emitting diodes (LEDs) connected through transparent electrodes with 3D Ag nanowires of different heights, as shown in **Figure 5E**. When a voltage was applied to the circuit, a distinct gradient of light intensity was observed depending on the height of the Ag nanowire. From the optical and electrical characterizations, it is important to note that this method can potentially avoid the trade-off between transmittance and resistance in transparent electrodes by providing an array of 3D Ag nanowires with high aspect ratios, which impart high conductivity but have little influence on light transmission.

A direct comparison between the transparent electrodes with the proposed 3D Ag nanowires with high aspect ratios and the previously reported transparent electrodes based on Ag nanowires/patterns is shown in **Figure S9**.^{32–40} In virtue of the narrow linewidth (400 nm) and tunable aspect ratio of the 3D nanowalls (up to 48 height/width), it was possible to avoid the trade-off between resistance and transmittance and to achieve improved performance.

In summary, we presented a straightforward and robust NFES method for the rapid fabrication of 3D nanofibrous architectures with high aspect ratios. Compared with other NFES techniques used to build 3D structures, which have been limited to micron-sized structures or special shapes (**Table S4**), this technique offers a method of nanoprinting 3D structures with precise, self-aligned walls into varied nanoarchitecture designs on demand. The addition of NaCl to the polymer solution increases the electrostatic attraction between the deposited fibers and the nanofiber jet, by providing the solution with high conductivity. This strong electrostatic attraction between the aerial jet and the previously deposited fibers was shown to enable effortless self-alignment that facilitates the construction of various nanoskyscraper designs, such as straight and curved nanowalls, nanojungle gyms, and nanobridges, by moving the collecting substrate on an X–Y stage

1
2
3 following a predesigned trajectory. The fabricated nanofibrous architectures had widths in the
4
5 range of 92 ± 3 to 239 ± 30 nm and lengths equal to 2 cm. With a width of 239 ± 30 nm, the height
6
7 could be controlled from 1.0 ± 0.2 to 11.4 ± 0.9 μm (aspect ratio: 4–48), while with a width of 92
8
9 ± 3 nm, the height was controllable from 0.8 ± 0.1 to 6.6 ± 0.1 μm (aspect ratio: 8–72). By adjusting
10
11 the number of 3D printed layers, the height of the nanostructure could be tuned precisely. This
12
13 gave facile control over the electrical resistance of 3D metal nanowires embedded in flexible
14
15 substrates and yielded high aspect ratios, while avoiding a trade-off with transmittance. Taken
16
17 together, this facile and precise NFES technique for 3D printing nanofibers possesses tremendous
18
19 potential for future applications in nanoelectronics, smart materials, and biomedical devices.
20
21
22
23
24
25
26
27
28
29
30
31
32
33
34
35
36
37
38
39
40
41
42
43
44
45
46
47
48
49
50
51
52
53
54
55
56
57
58
59
60

FIGURES

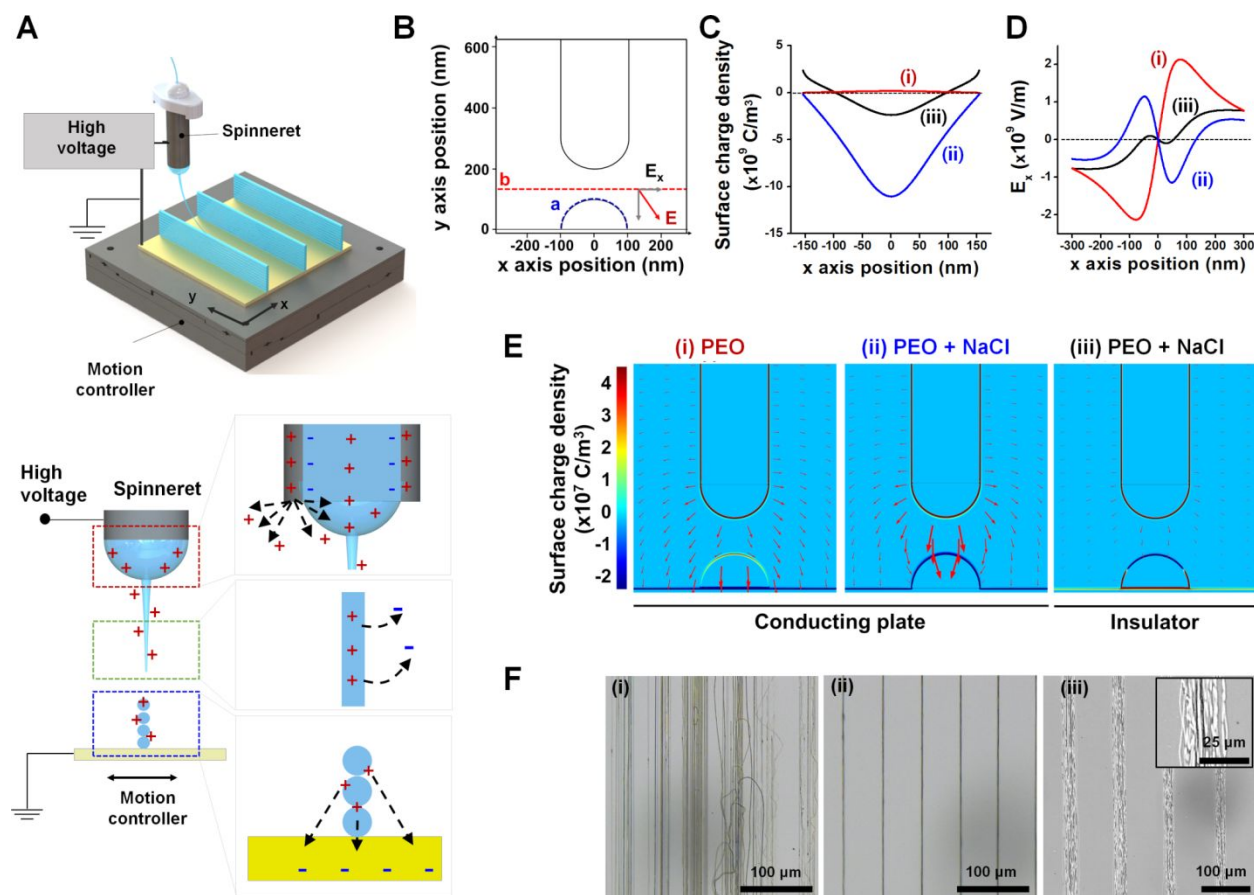


Figure 1. High-resolution near-field electrospinning (NFES) 3D nanoprining for the fabrication of 3D nanofibrous structures. (A) Schematic presentation of the experimental setup. Charge carriers are generated in the polymer solution via charge emission with a conducting spinneret, followed by charge dissociation from the bulk liquid during the flight phase and after deposition on the collecting electrode, based on surface contact and inverse corona discharges. (B) 2D schematic diagram depicting the geometry used in the numerical simulation. (C) Surface charge density at surface “a” and (D) x-component of the electric field strength along line “b” for the three cases in (E); field focusing is observed for case (ii). (E) Simulation results for printing (i) pure polyethylene oxide (PEO) solution and (ii) PEO + NaCl solution on a conducting plate, and (iii) PEO + NaCl solution on an insulating surface. Electric field arrows and surface charge density

1
2
3 contours are shown. (F) Optical images of the 3D printed nanofibers corresponding to the three
4 cases in (E). (i) Pure PEO solution on a conductive plate: no 3D stacking owing to repulsion
5 between the electrospun jet and the deposited fibers due to their high residual charge. (ii) PEO +
6 NaCl solution on a conductive plate: considerably higher precision nanofiber alignment and
7 stacking owing to the negative charge of the deposited fibers. (iii) PEO + NaCl solution on
8 insulating material: misaligned stacked nanofibers owing to the partial negative charge on the as
9 deposited fibers due to reduced charge dissipation.
10
11
12
13
14
15
16
17
18
19
20
21
22
23
24
25
26
27
28
29
30
31
32
33
34
35
36
37
38
39
40
41
42
43
44
45
46
47
48
49
50
51
52
53
54
55
56
57
58
59
60

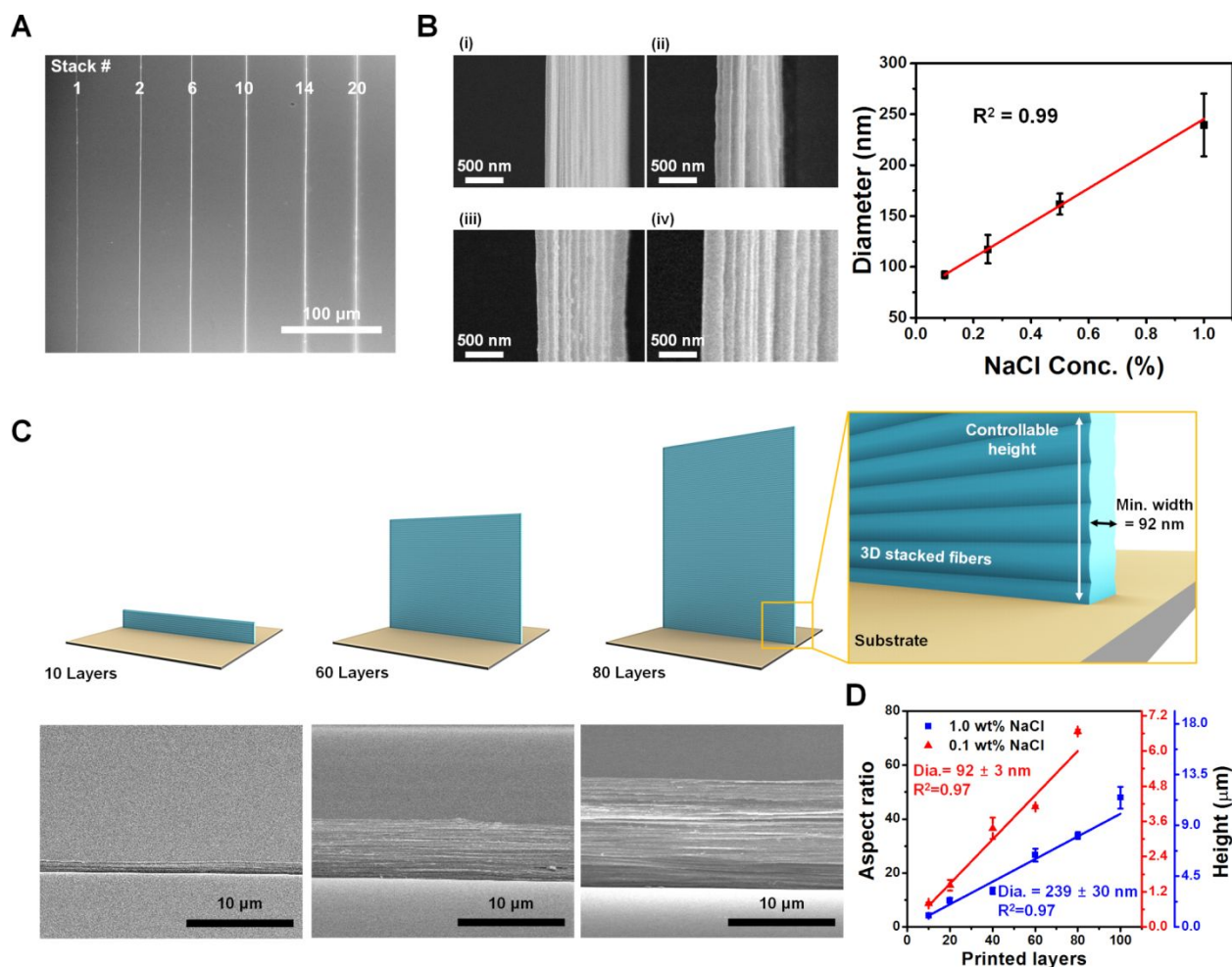


Figure 2. Precise printing control of 3D nanofibrous structures. **(A)** Scanning electron microscopy (SEM) image (top view) of constructed nanowalls with different numbers of layers. **(B)** Nanowall diameter depending on the NaCl concentration of the PEO solution: **(i)** 0.1 wt% (92 ± 3 nm), **(ii)** 0.25 wt% (117 ± 14 nm), **(iii)** 0.5 wt% (161 ± 10 nm), and **(iv)** 1 wt% (239 ± 30 nm). **(v)** Linear relationship between the NaCl concentration and the fiber diameter ($R^2 = 0.99$). **(C)** Schematic and SEM images (side views) of 3D printed nanowalls consisting of different numbers of nanofiber layers. **(D)** Linear relationship between the nanowall height and the number of stacked layers ($R^2 = 0.97$).

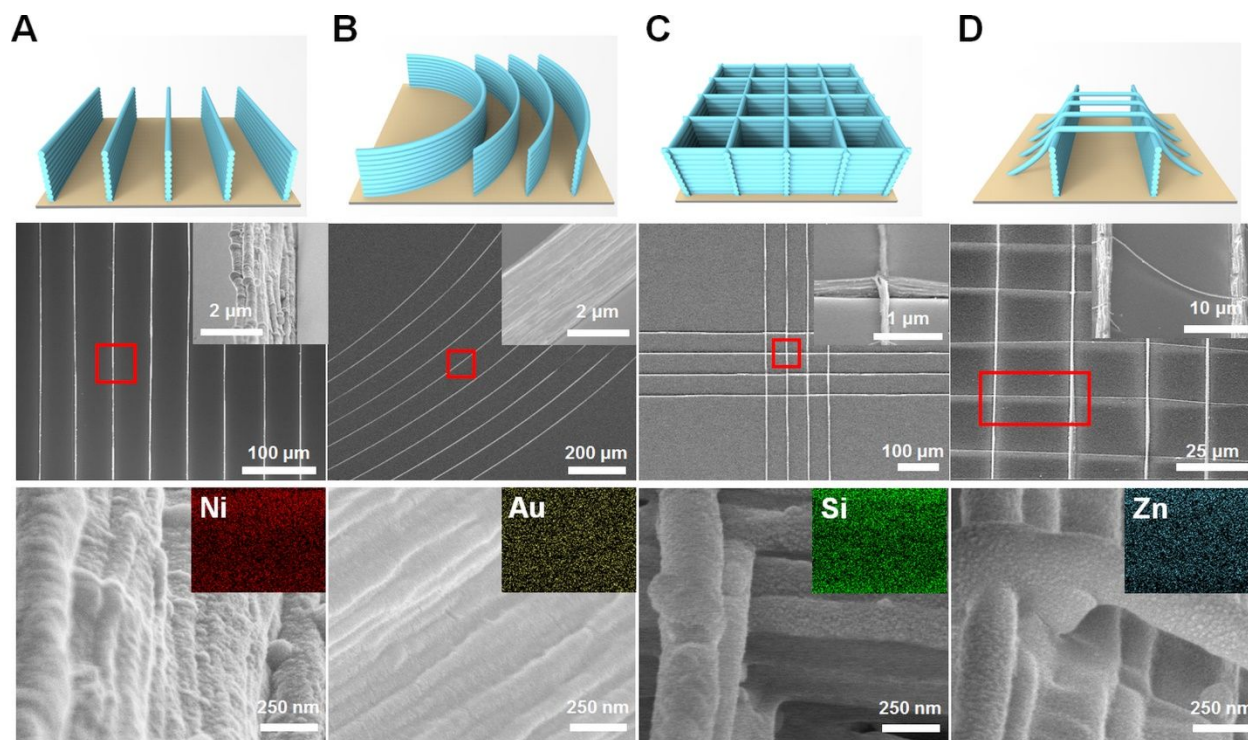


Figure 3. Schematics, scanning electron microscopy (SEM) images, and energy dispersive X-ray spectroscopy (EDS) maps of various 3D printed nanoarchitectures coated with different functional materials (Ni, Au, SiO₂, and ZnO). **(A)** Straight Ni nanowalls comprising 40 nanofiber layers (distance between walls: 50 μm). **(B)** Curved Au nanowalls comprising 40 nanofiber layers (distance between walls: 100 μm). **(C)** SiO₂ grid pattern comprising 40-layer high nanowalls (distance between walls: 50 μm). **(D)** ZnO nanobridges comprising 40-layer high nanowalls (distance between walls: 25 μm) connected by single fibers suspended between the nanowalls (distance between suspended fibers: 25 μm). All fibers were fabricated under the same NFES conditions (described in the experimental methods) with different G-codes for the stage movement.

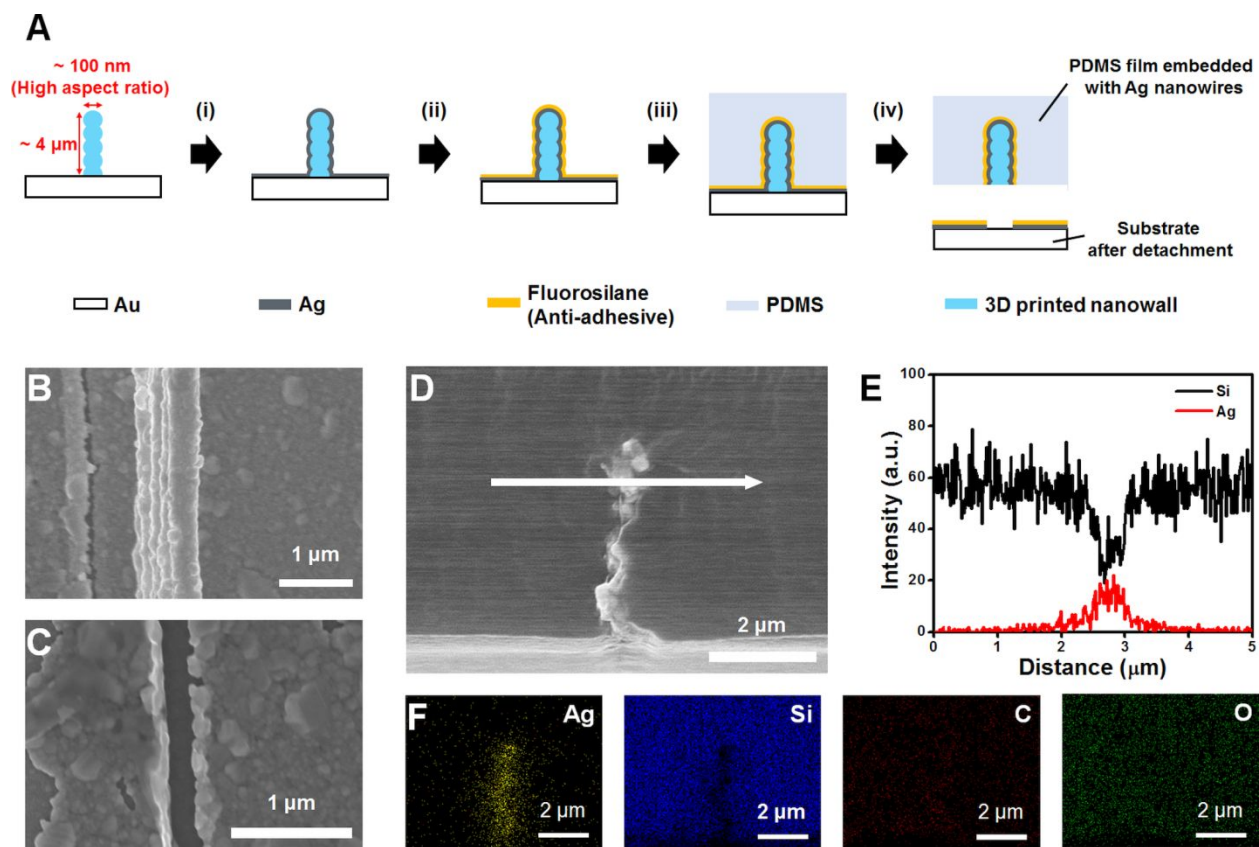


Figure 4. Fabrication of transparent electrodes embedded with 3D Ag nanowire architectures using 3D printed nanofibers. (A) Scheme showing the fabrication of a conductive polydimethylsiloxane (PDMS) film embedded with Ag nanowires: (i) Ag sputtering, (ii) anti-adhesive coating, (iii) PDMS coating, and (iv) detachment. (B–D) Scanning electron microscopy (SEM) images of the transfer process: (B) top view of the PDMS film embedded with Ag nanowires, (C) top view of the substrate after the transfer of Ag nanowires, and (D) cross-sectional view of the PDMS film embedded with Ag nanowires. SEM–energy dispersive X-ray spectroscopy (SEM–EDS) (E) line scan and (F) elemental mapping of the PDMS film embedded with 3D Ag nanowires.

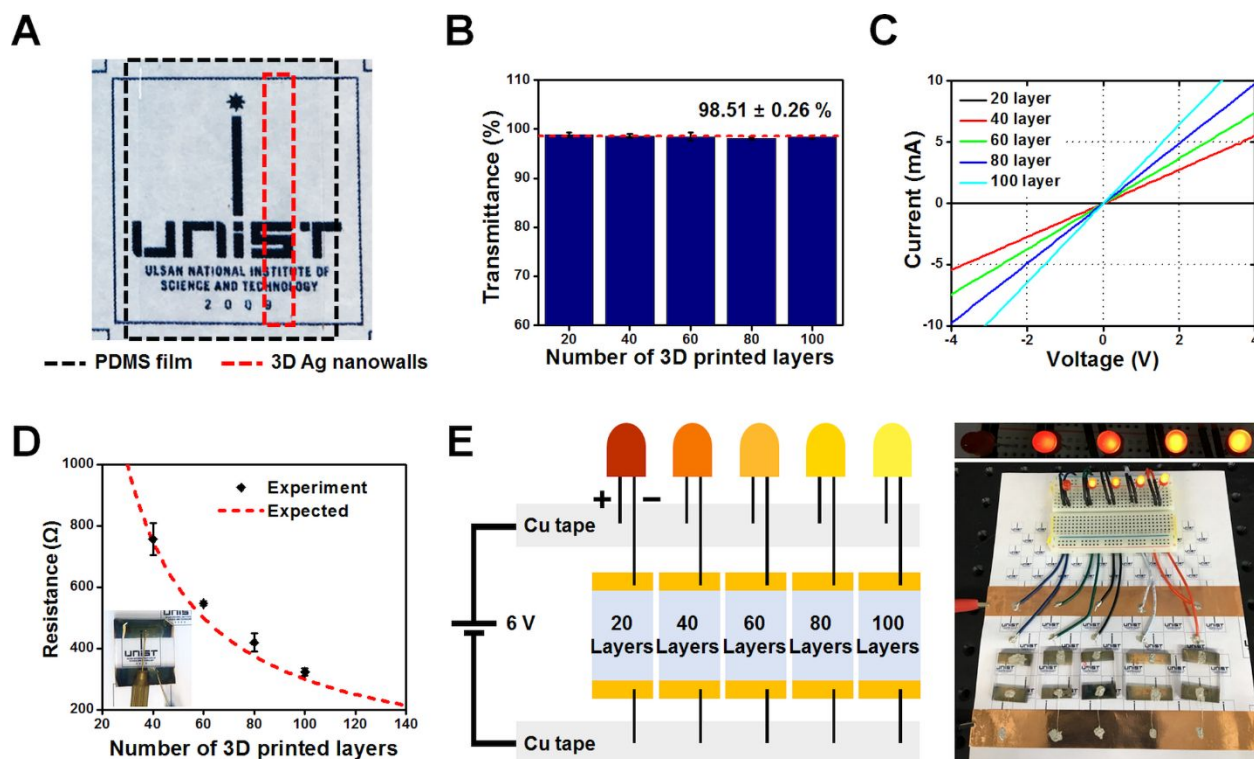


Figure 5. Optical and electrical characterization of transparent electrodes. (A) Optical image of transparent polydimethylsiloxane (PDMS) electrode with embedded 3D Ag nanowires. (B) Transmittance of the transparent electrodes depending on the number of 3D printed layers of Ag nanowires (20–100 layers). The average transmittance was 98.5%. (Note that this does not include the transmittance of the substrate.) (C) Current–voltage (I–V) curve of PDMS transparent electrodes embedded with multilayered 3D Ag nanowires (20–100 layers). All electrodes yielded stable ohmic contacts. (D) Experimental and expected resistances of the transparent electrodes with 40–100-layer high embedded Ag nanowires. (E) Setup to identify the resistance tunability of the transparent electrodes based on a light emitting diode (LED) intensity comparison.

ASSOCIATED CONTENT

Supporting Information. The following files are available free of charge.

Detailed description of experimental methods, additional figures and a table (PDF)

Effect of salt concentration on 3D printing of NF (AVI)

Electrostatic attraction between deposited fibers and polymer solution (AVI)

AUTHOR INFORMATION

Corresponding Author

*E-mail: ykcho@unist.ac.kr

Present Addresses

†Department of Chemical Engineering, Pohang University of Science and Technology, 77
Cheongam-ro, Nam-gu, Pohang 37673, Republic of Korea

Author Contributions

+These authors contributed equally.

The manuscript was written based on contributions from all authors. All authors have approved the final version of the manuscript.

Notes

The authors declare no competing financial interests.

ACKNOWLEDGMENT

The work was supported by the Institute for Basic Science of Korea (IBS-R020-D1).

ABBREVIATIONS

2D, two-dimensional; 3D, three-dimensional; CCD, charge-coupled device; DC, direct current; DI, deionized; EDS, energy-dispersive X-ray spectroscopy; EHD printing, electrohydrodynamic printing; LED, light emitting diodes; MES, melt electrospinning; NFES, near-field electrospinning; PEO, polyethylene oxide; PDMS, polydimethylsiloxane; RPM, revolutions per minute; SEM, scanning electron microscopy; UV-vis, ultraviolet visible.

REFERENCES

- (1) Xue, J.; Wu, T.; Dai, Y.; Xia, Y. *Chem. Rev.* **2019**, *119* (8), 5298–5415.
- (2) Sun, D.; Chang, C.; Li, S.; Lin, L. *Nano Lett.* **2006**, *6* (4), 839–842.
- (3) He, X.-X.; Zheng, J.; Yu, G.-F.; You, M.-H.; Yu, M.; Ning, X.; Long, Y.-Z. *J. Phys. Chem. C.* **2017**, *121* (16), 8663–8678.
- (4) Bisht, G. S.; Canton, G.; Mirsepassi, A.; Kulinsky, L.; Oh, S.; Dunn-Rankin, D.; Madou, M. J. *Nano Lett.* **2011**, *11* (4), 1831–1837.
- (5) Liu, Z. H.; Pan, C. T.; Yen, C. K.; Lin, L. W.; Huang, J. C.; Ke, C. A. *Appl. Surf. Sci.* **2015**, *346*, 291–301.
- (6) Chang, C.; Tran, V. H.; Wang, J.; Fuh, Y.-K.; Lin, L. *Nano Lett.* **2010**, *10* (2), 726–731.
- (7) Fuh, Y.-K.; Ye, J.-C.; Chen, P.-C.; Ho, H.-C.; Huang, Z.-M. *ACS Appl. Mater. Interfaces* **2015**, *7* (31), 16923–16931.
- (8) Fuh, Y.-K.; Wu, Y.-C.; He, Z.-Y.; Huang, Z.-M.; Hu, W.-W. *Mater. Sci. Eng., C* **2016**, *62*, 879–887.
- (9) Zhang, B.; He, J.; Li, X.; Xu, F.; Li, D. *Nanoscale* **2016**, *8* (34), 15376–15388.
- (10) Brown, T. D.; Dalton, P. D.; Hutmacher, D. W. *Adv. Mater.* **2011**, *23* (47), 5651–5657.

- (11) He, J.; Xia, P.; Li, D. *Biofabrication* **2016**, 8 (3), 035008.
- (12) He, J.; Xu, F.; Dong, R.; Guo, B.; Li, D. *Biofabrication* **2017**, 9 (1), 015007.
- (13) Visser, J.; Melchels, F. P. W.; Jeon, J. E.; van Bussel, E. M.; Kimpton, L. S.; Byrne, H. M.; Dhert, W. J. A.; Dalton, P. D.; Hutmacher, D. W.; Malda, J. *Nat. Commun.* **2015**, 6, 6933.
- (14) Wunner, F. M.; Wille, M.-L.; Noonan, T. G.; Bas, O.; Dalton, P. D.; De-Juan-Pardo, E. M.; Hutmacher, D. W. *Adv. Mater.* **2018**, 30 (20), 1706570.
- (15) Zeng, J.; Wang, H.; Lin, Y.; Zhang, J.; Liang, F.; Fang, F.; Yang, F.; Wang, P.; Zhu, Z.; Chen, X.; Chen, X.; Wang, Z.; Cai, N.; Tang, Y.; Wu, P. *Microfluid. Nanofluid.* **2018**, 22 (2), 23.
- (16) Huang, Y.; Bu, N.; Duan, Y.; Pan, Y.; Liu, H.; Yin, Z.; Xiong, Y. *Nanoscale* **2013**, 5 (24), 12007–12017.
- (17) He, J.; Xu, F.; Cao, Y.; Liu, Y.; Li, D. *J. Phys. D: Appl. Phys.* **2016**, 49 (5), 055504.
- (18) Lee, M.; Kim, H.-Y. *Langmuir* **2014**, 30 (5), 1210–1214.
- (19) Kim, H.-Y.; Lee, M.; Park, K. J.; Kim, S.; Mahadevan, L. *Nano Lett.* **2010**, 10 (6), 2138–2140.
- (20) Zhao, S.; Zhou, Q.; Long, Y.-Z.; Sun, G.-H.; Zhang, Y. *Nanoscale* **2013**, 5 (11), 4993–5000.
- (21) Choi, W.; Kim, G. H.; Shin, J. H.; Lim, G.; An, T. *Nanoscale Res. Lett.* **2017**, 12 (1), 610.
- (22) Kim, G. H.; Nam, H.; Choi, W.; An, T.; Lim, G. *Adv. Mater. Interfaces* **2018**, 5 (5), 1701204.
- (23) Park, S. M.; Kim, D. S. *Adv. Mater.* **2015**, 27 (10), 1682–1687.
- (24) Luo, G.; Teh, K. S.; Liu, Y.; Zang, X.; Wen, Z.; Lin, L. *ACS Appl. Mater. Interfaces* **2015**, 7 (50), 27765–27770.
- (25) Collins, G.; Federici, J.; Imura, Y.; Catalani, L. H. *J. Appl. Phys.* **2012**, 111 (4), 044701.

- (26) Sun, B.; Long, Y.-Z.; Yu, F.; Li, M.-M.; Zhang, H.-D.; Li, W.-J.; Xu, T.-X. *Nanoscale* **2012**, 4 (6), 2134–2137.
- (27) Vong, M.; Speirs, E.; Klomkliang, C.; Akinwumi, I.; Nuansing, W.; Radacsi, N. *RSC Adv.* **2018**, 8 (28), 15501–15512.
- (28) Reis, T. C.; Correia, I. J.; Aguiar-Ricardo, A. *Nanoscale* **2013**, 5 (16), 7528–7536.
- (29) Ahirwal, D.; Hébraud, A.; Kádár, R.; Wilhelm, M.; Schlatter, G. *Soft Matter* **2013**, 9 (11), 3164–3172.
- (30) An, B. W.; Kim, K.; Lee, H.; Kim, S.-Y.; Shim, Y.; Lee, D.-Y.; Song, J. Y.; Park, J.-U. *Adv. Mater.* **2015**, 27 (29), 4322–4328.
- (31) Yoon, J.-W.; Noh, B.-I.; Jung, S.-B. *Microelectron. Reliab.* **2014**, 54 (2), 410–416.
- (32) Kang, M. G.; Kim, M. S.; Kim, J.; Guo, L. J. *Adv. Mater.* **2008**, 20, (23), 4408–4413.
- (33) De, S.; Higgins, T. M.; Lyons, P. E.; Doherty, E. M.; Nirmalraj, P. N.; Blau, W. J.; Boland, J. J.; Coleman, J. N. *ACS Nano* **2009**, 3 (7), 1767–1774.
- (34) Jiu, J.; Nogi, M.; Sugahara, T.; Tokuno, T.; Araki, T.; Komoda, N.; Suganuma, K.; Uchida, H.; Shinozaki, K. *J. Mater. Chem.* **2012**, 22 (44), 23561–23567.
- (35) van de Groep, J.; Spinelli, P.; Polman, A. *Nano Lett.* **2012**, 12 (6), 3138–3144.
- (36) Hong, S.; Yeo, J.; Kim, G.; Kim, D.; Lee, H.; Kwon, J.; Lee, H.; Lee, P.; Ko, S. H. *ACS Nano* **2013**, 7 (6), 5024–5031.
- (37) Park, J.; Hwang, J. *J. Phys. D: Appl. Phys.* **2014**, 47 (40), 405102.
- (38) Schneider, J.; Rohner, P.; Thureja, D.; Schmid, M.; Galliker, P.; Poulikakos, D. *Adv. Funct. Mater.* **2016**, 26 (6), 833–840.
- (39) Jang, Y.-R.; Chung, W.-H.; Hwang, Y.-T.; Hwang, H.-J.; Kim, S.-H.; Kim, H.-S. *ACS Appl. Mater. Interfaces* **2018**, 10 (28), 24099–24107.

1
2
3
4
5
6
7
8
9
10
11
12
13
14
15
16
17
18
19
20
21
22
23
24
25
26
27
28
29
30
31
32
33
34
35
36
37
38
39
40
41
42
43
44
45
46
47
48
49
50
51
52
53
54
55
56
57
58
59
60

(40) Jiang, Z.; Fukuda, K.; Xu, X.; Park, S.; Inoue, D.; Jin, H.; Saito, M.; Osaka, I.; Takimiya, K.; Someya, T. *Adv. Mater.* **2018**, *30* (26), 1707526.

For Table of Contents Only

**Self-aligned,
template-free,
nanoscale 3D printing**